Positron Emission Tomography Imaging of Regional Pulmonary Perfusion and Ventilation

Guido Musch and Jose G. Venegas

Department of Anesthesia and Critical Care, Massachusetts General Hospital and Harvard Medical School, Boston, Massachusetts

Positron emission tomography (PET) imaging is a noninvasive, quantitative method to assess pulmonary perfusion and ventilation *in vivo*. The core of this article focuses on the use of [^{13}N]nitrogen ($^{13}N_2$) and PET to assess regional gas exchange. Regional perfusion and shunt can be measured with the $^{13}N_2$–saline bolus infusion technique. A bolus of $^{13}N_2$, dissolved in saline solution, is injected intravenously at the start of a brief apnea, while the tracer kinetics in the lung is measured by a sequence of PET frames. Because of its low solubility in blood, virtually all $^{13}N_2$ delivered to aerated lung regions diffuses into the alveolar airspace, where it accumulates in proportion to regional perfusion during the apnea. In contrast, lung regions that are perfused but are not aerated and do not exchange gas (i.e., "shunting" units) do not retain $^{13}N_2$ during apnea and the tracer concentration drops after the initial peak. Accurate estimates of regional perfusion and regional shunt can be derived by applying a mathematical model to the pulmonary kinetics of a $^{13}N_2$–saline bolus. When breathing is resumed, specific alveolar ventilation can be calculated from the tracer washout rate, because $^{13}N_2$ is eliminated almost exclusively by ventilation. Because of the rapid elimination of the tracer, $^{13}N_2$ infusion scans can be followed by $^{13}N_2$ inhalation scans that allow determination of regional gas fraction. This article describes insights into the pathophysiology of acute lung injury, pulmonary embolism, and asthma that have been gained by PET imaging of regional gas exchange.

Keywords: adult respiratory distress syndrome; asthma; emission-computed tomography; nitrogen isotopes; pulmonary embolism; pulmonary gas exchange

Novel imaging methods have substantially expanded the ability to assess and quantify regional lung function compared with classical ventilation–perfusion scanning with inhaled ^{133}Xe and ^{99m}Tc-macroaggregated albumin. This article describes the experimental and clinical applications of positron emission tomography (PET) to the study of regional lung gas exchange. PET entails the administration of a radioisotope that decays by emitting a positron. The positron annihilates with an electron into two 511-keV antiparallel photons. The two annihilation photons travel through the object that is being scanned and are detected by external crystals arranged in rings around the object. By coincidence detection of annihilation photons, a three-dimensional map of the radioactivity, which is proportional to the concentration of the radioisotope within the object, can be reconstructed and displayed as an image.

(*Received in original form August 8, 2005; accepted in final form September 26, 2005*)

Supported by National Institutes of Health grants HL-68011 and GM-07592 and by a research grant from the Foundation for Anesthesia Education and Research–American Society of Critical Care Anesthesiologists.

Correspondence and request for reprints should be addressed to Guido Musch, M.D., Department of Anesthesia and Critical Care, CLN 309, Massachusetts General Hospital, 55 Fruit Street, Boston, MA 02114. E-mail: gmusch@partners.org

The color figures for this article are on pp. 508–509.

Proc Am Thorac Soc Vol 2. pp 522–527, 2005
DOI: 10.1513/pats.200508-088DS
Internet address: www.atsjournals.org

PET IMAGING OF [^{13}N]NITROGEN

[^{13}N]nitrogen ($^{13}N_2$) is a positron emitter with a half-life of 9.96 min. The low solubility of nitrogen in body fluids and tissues (partition coefficient: $\lambda_{water/air} = 0.015$ at 37°C) entails that virtually all $^{13}N_2$ infused intravenously in saline solution evolves into the alveolar airspace at first pass, whereas inhaled $^{13}N_2$ remains confined to the airspace. Analysis of the intrapulmonary concentration of $^{13}N_2$ can be used to assess regional perfusion, shunt, aeration, ventilation, and gas trapping.

$^{13}N_2$–Saline Bolus Infusion Technique

This technique represents a modification of the constant rate intravenous infusion of $^{13}N_2$ in saline originally described by Rhodes and coworkers (1, 2) to measure regional ventilation–perfusion ratio. In this technique, a bolus of $^{13}N_2$ gas dissolved in saline solution ($\sim$ 30 ml) is infused intravenously over the initial 3 to 5 s of a 30- to 60-s apnea (3, 4). Simultaneously with the start of the $^{13}N_2$–saline infusion, the acquisition of a series of sequential PET frames is initiated to measure the pulmonary kinetics of $^{13}N_2$ during apnea and the ensuing 3 min of ventilation after breathing is resumed (tracer washout). Because of the low solubility of gaseous nitrogen in blood and tissues, the pulmonary kinetics of infused $^{13}N_2$ during apnea is different in gas-exchanging and in non–gas-exchanging units (5–7). Indeed, on arrival into the pulmonary capillaries of alveolar units that are perfused and aerated, virtually all infused $^{13}N_2$ diffuses into the alveolar airspace at first pass, where it accumulates in proportion to regional perfusion. Perfusion to aerated regions can be calculated from the plateau tracer activity during apnea (4). In contrast, units that are perfused but are not aerated, and cannot exchange gas between their capillary blood and alveolar airspace (i.e., "shunting" units), do not retain $^{13}N_2$. Accordingly, $^{13}N_2$ kinetics during apnea in lung regions that contain shunting units shows an early peak of tracer activity, corresponding to the arrival of the bolus of tracer through the pulmonary circulation, followed by an exponential decrease toward a plateau (Figure 1). This kinetic behavior reflects the fact that $^{13}N_2$ is carried through shunting units by the pulmonary blood flow, whereas it is retained in the airspace of units that are aerated (Figure 2 [p. 508]). Accurate estimates of regional perfusion and regional shunt fraction can be derived by applying a mathematical model to the pulmonary kinetics of a $^{13}N_2$–saline bolus, measured by PET during apnea (5, 6). This tracer kinetics model lumps the alveolar units within a region into two parallel compartments. One compartment represents units that are perfused and aerated, the other represents units that are perfused but not aerated (i.e., fluid-filled, consolidated, or collapsed) and do not exchange gas. Because the measurement of shunt fraction with the $^{13}N_2$–saline bolus technique is obtained during apnea, it is not affected by the presence of units with very low ventilation but preserved aeration (i.e., "gas trapping"). These units retain $^{13}N_2$ during apnea because they are aerated and, consequently, do not contribute to the measured shunt, despite the fact that their ventilation is very low.

When breathing is resumed at the end of apnea, specific alveolar ventilation (i.e., alveolar ventilation per unit of gas

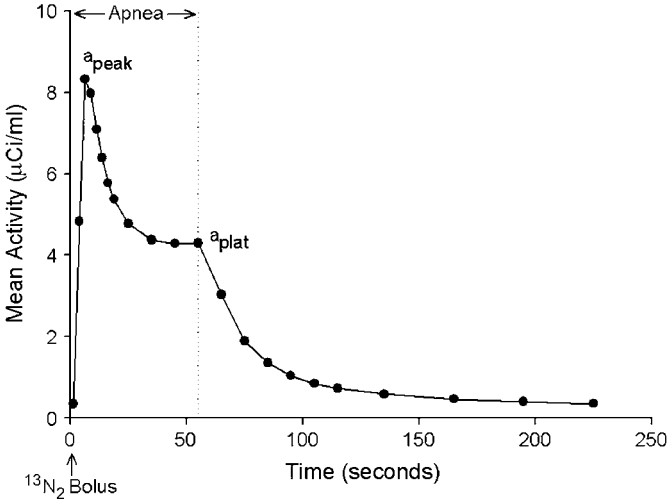

Figure 1. Pulmonary kinetics of infused [^{13}N]nitrogen ($^{13}N_2$) measured by positron emission tomography (PET) in an animal after saline lung lavage. After a 3-s intravenous infusion of a bolus of $^{13}N_2$ dissolved in saline solution, PET images were acquired during 60 s of apnea (*left of vertical dotted line*) and 3 min of ensuing ventilation (*right of vertical dotted line*). $^{13}N_2$ kinetics during apnea shows an early peak of tracer activity (a_{peak}), corresponding to arrival of the bolus of tracer through the pulmonary circulation, followed by a decrease toward a plateau (a_{plat}). This decrease in activity is consistent with the presence of shunting units, which do not retain $^{13}N_2$ during apnea, whereas the plateau reflects the retention of $^{13}N_2$ in units that are perfused and aerated. Specific alveolar ventilation of perfused units is calculated from the washout rate of tracer, after breathing is resumed. Reprinted by permission from Reference 29.

volume) of lung regions that, being perfused and aerated, retained tracer during apnea can be calculated from the washout rate of $^{13}N_2$, because infused $^{13}N_2$ is eliminated from aerated regions almost exclusively by ventilation (8). In the presence of uniform ventilation within the region, the washout of tracer is accurately described by a single compartment model, manifested by single exponential washout kinetics (4). In contrast, in the presence of intraregional heterogeneity of ventilation, the turnover rate derived from the initial part of the washout represents a perfusion-weighted average of the turnover rates of alveolar gas in units within the region (9). A model with a fast- and a slow-ventilating compartment can be used to estimate turnover rates of alveolar gas in units with, respectively, normal ventilation and hypoventilation. Furthermore, because the distribution of tracer at the start of the washout is proportional to regional perfusion to aerated units, the respective fraction of perfusion to the fast- and slow-ventilating compartments within the region can be estimated. This assessment of intraregional heterogeneity is essential for accurate description of ventilation–perfusion distributions in disease states characterized by acute bronchoconstriction (10). In these states, the lung volume elements (voxels) showing intraregional heterogeneity represent a considerable fraction of the lung, in contrast to the predominant single compartment behavior of normal lungs (4).

The $^{13}N_2$–saline bolus infusion technique can be used to quantitatively assess heterogeneity of regional ventilation–perfusion ratio even when such heterogeneity occurs at length scales smaller than the imaging resolution. The spatial resolution of PET ($\sim$1 cm) is indeed lower than that of computed tomography (CT) or magnetic resonance imaging (MRI). As resolution increases, however, the effect of misregistration of ventilation and perfusion images and artifacts caused by lung motion can contribute disproportionately to the measured heterogeneity of ventilation–perfusion ratio. Studies demonstrate that, despite the inability of PET to quantify ventilation and perfusion at very small scales, the $^{13}N_2$–saline bolus technique can be used to recover ventilation–perfusion heterogeneity occurring at scales lower than the imaging resolution, because the kinetic information derived from the sequence of PET frames can be used to estimate the functional effect of heterogeneity present within the resolution volume (10). This characteristic partially compensates for the limited spatial resolution of PET.

Kreck and coworkers (11) reported ventilation–perfusion distributions obtained by imaging Xe washin with CT. Because the tracer is delivered by inhalation rather than by perfusion, inhaled Xe yields low signal-to-noise ratio in units with a ventilation–perfusion ratio that approaches zero, which are the units that contribute the most to the hypoxemia observed in disease states characterized by shunt. Eberle and coworkers (12) estimated alveolar oxygen concentration by measuring, with MRI, the longitudinal relaxation time constant of hyperpolarized ^{3}He, which depends on the local concentration of paramagnetic oxygen, in normal pigs. They showed good correlation with end-tidal oxygen fraction. Their analysis was limited, however, by the low signal-to-noise ratio that required use of large regions of interest. Rizi and coworkers (13) recently showed that regional alveolar P_{O_2}, estimated by MRI of hyperpolarized ^{3}He, could be combined with measured blood gases to yield realistic ventilation–perfusion distributions. Petersson and coworkers (14) used single-photon emission computed tomography (SPECT) imaging of inhaled Technegas and infused macroaggregated albumin to assess regional perfusion and ventilation in humans. They showed that ventilation–perfusion distributions obtained by SPECT were consistent with those obtained by multiple inert gas elimination in healthy lungs. Rhodes and coworkers (1, 2) used a constant rate intravenous infusion of $^{13}N_2$ and PET to estimate regional ventilation–perfusion ratio in humans. Compared with the constant rate infusion of $^{13}N_2$, the bolus infusion technique minimizes the need for correction for tracer activity in the blood and does not require a measurement of pulmonary blood volume. Furthermore, the bolus infusion technique does not saturate the PET scanner with radioactivity accumulated in lung regions with gas trapping or very low ventilation, in contrast to the constant rate infusion technique in which $^{13}N_2$ progressively accumulates in those regions. Differently from the $^{13}N_2$–saline technique, other methods for functional lung imaging have not yet been shown to yield quantitative measurements of regional gas exchange that correlate with arterial blood gases in the setting of pulmonary disease states characterized by impairment of gas exchange. Instead, the authors found high correlation between blood gas tensions estimated with the $^{13}N_2$–saline bolus infusion technique and those measured in arterial blood (10).

Additional advantages of the $^{13}N_2$–saline bolus infusion technique include its ability to assess regional perfusion, shunt, and ventilation of perfused units with a single administration of tracer and low radiation exposure to the subject ($\sim$0.2 mSv/administration) and its potential to be combined with PET measurements of other functional and metabolic variables, given the short half-life of $^{13}N_2$ and, more important, the fact that infused $^{13}N_2$ is rapidly eliminated from the lung when ventilation is resumed. These characteristics make this method suitable for future clinical applications in a variety of lung diseases. In particular, this technique is ideally suited to detect and quantify regional hypoventilation and gas trapping, which can occur in asthma or in chronic obstructive pulmonary disease, because $^{13}N_2$ is delivered to poorly ventilated units through the pulmonary bloodstream and is retained locally even after breathing is resumed (15).

Regions with severe hypoventilation appear as regions of tracer retention on PET frames acquired at the end of the washout phase (Figure 3 [p. 509]). Methods based instead on the inhalation of tracer cannot directly reveal the occurrence of gas trapping because inhaled tracer is not deposited in the airspace distal to a severely constricted airway.

Current limitations of this technique include the cost and limited availability of on-site cyclotrons to produce $^{13}N_2$, the practical difficulty of producing a high-yield solution of $^{13}N_2$ in saline, and the need for a brief apnea after administration of the tracer. One should note, however, that the distribution of $^{13}N_2$ within the lung, and hence the registration of regional blood flow, occurs during the first few seconds of apnea. Therefore, the perfusion measurement is only minimally affected by possible changes in blood flow occurring during the remainder of the apnea. To prevent alveolar derecruitment during apnea and to ensure that the lung volume at which measurements of perfusion and shunt are obtained is similar to the mean lung volume at which ventilation is measured during washout, the apnea is performed at mean lung volume (determined by averaging lung volume, measured with impedance plethysmography, over several breaths before the injection of $^{13}N_2$–saline) in spontaneously breathing subjects or at an airway pressure equal to mean airway pressure in mechanically ventilated subjects. Another limitation of this technique is that ventilation of regions that are poorly perfused is not quantifiable with the infusion of $^{13}N_2$ because the tracer is distributed by the pulmonary blood flow. To specifically target these regions, methods based on imaging the kinetics of inhaled tracer are used.

$^{13}N_2$ Inhalation Technique

Because of its low solubility, inhaled $^{13}N_2$ remains virtually confined to the alveolar airspace and, after equilibration with the alveolar gas, tracer activity within a region of lung is proportional to the fraction of the region's volume occupied by gas. Regional gas fraction is calculated by dividing regional specific tracer activity (i.e., activity per unit of lung volume, expressed in μCi/ml), measured with PET (Figure 2 [p. 508]), by the activity of a 1-ml sample of inhaled gas obtained after equilibration. Regional gas volume is calculated as the product of regional lung volume and gas fraction.

$^{13}N_2$ inhalation PET scans can be performed by having the subject breathe from a closed circuit system, equipped with a carbon dioxide absorber and supplemental oxygen, in which $^{13}N_2$ gas has been introduced (7, 9). After PET frames of equilibrated $^{13}N_2$ are acquired, inhalation from the breathing system is switched to tracer-free gas, while PET imaging continues as $^{13}N_2$ is eliminated from the alveolar airspace by ventilation (washout). Estimates of specific ventilation can be derived from the washout rate of inhaled $^{13}N_2$ (9, 16). The washout rate of inhaled $^{13}N_2$ represents specific ventilation of units that are aerated and ventilated, including dead space ventilation. The short half-life of $^{13}N_2$ and, more important, the rapid elimination of $^{13}N_2$ by ventilation with tracer-free gas allow $^{13}N_2$ infusion and inhalation scans to be performed in sequence within a relatively short period of time ($\sim$ 10 min).

$^{13}N_2$ can also be administered by constant rate inhalation through a custom apparatus connected to a regular ventilator operated in open circuit (16). This technical modification does not require a closed circuit system. The analysis of $^{13}N_2$ washout kinetics is performed with the same single or double compartment models that have been used to estimate ventilation from the washout kinetics of infused $^{13}N_2$ (10) or of $^{13}N_2$ equilibrated by rebreathing (9, 17). The radiation dose that was administered to animals with this open circuit system (16) is more than fivefold greater, however, than that which was administered to humans to quantify ventilation to gas-exchanging regions after infusion of $^{13}N_2$ (4).

PET IMAGING OF PULMONARY BLOOD FLOW AND LUNG WATER WITH $H_2{}^{15}O$

In addition to the $^{13}N_2$–saline bolus infusion technique, a second method that allows assessment of regional pulmonary blood flow is based on the intravenous administration of $H_2{}^{15}O$ as the radiotracer (18, 19). This method is based on a single compartment model of the distribution of tracer and relies on two basic assumptions: the tracer is biologically inert, and the tracer is freely and rapidly diffusible in the lung, so that the concentration of tracer in the pulmonary venous blood that flows out of a region is equal to the concentration of tracer in the tissue, divided by the tissue–blood partition coefficient of the tracer (i.e., the tracer leaves the lung at equilibrium with lung tissue). This assumption has been demonstrated to hold even for very high values of regional pulmonary blood flow (18).

In this technique, $H_2{}^{15}O$ is infused intravenously at a constant rate during 20 s of apnea. A PET scan of the lung is acquired to measure regional tissue activity during the infusion of $H_2{}^{15}O$, whereas the "input function" to the lungs is derived from the activity of the blood perfusing the lungs during the scan, measured either by constant rate sampling of pulmonary arterial blood (18) or by counting, with PET, the activity in a region of interest corresponding to the right heart (19). At the end of the PET scan, ventilation is resumed and the remaining $H_2{}^{15}O$ is injected. After allowing 4 min for $H_2{}^{15}O$ to equilibrate throughout body tissues, a second PET scan is acquired over 5 min while blood activity is measured in samples taken at 30-s intervals during the scan. The lung tissue activity derived from the second scan and the corresponding blood activity are used to calculate the regional tissue–blood partition coefficient for $H_2{}^{15}O$. Indeed, because the lung is not uniformly inflated, the tissue–blood partition coefficient needs to be determined on a regional basis. The partition coefficient and the lung tissue and pulmonary arterial blood activities, measured during the first PET scan, are used to calculate regional pulmonary blood flow from the equation that describes the mathematical model of tracer distribution (18). Regional lung water can be measured by normalizing lung tissue activity at equilibrium by the activity of blood water, measured from the samples collected during the second scan. The main advantage of the $H_2{}^{15}O$ technique is that it allows accurate and repeatable (half-life of ^{15}O: 2.05 min) measurements of pulmonary blood flow and lung water *in vivo*. The accuracy of the pulmonary blood flow measurement is decreased, however, in regions of lung with high blood flow and low density (20). Intravascular lung water can be calculated by taking a PET scan and measuring blood activity after inhalation of ^{11}C- or ^{15}O-carbon monoxide, which binds to hemoglobin with high affinity. Extravascular lung water can then be obtained by subtracting intravascular water from regional water (20). In conditions characterized by increased pulmonary vascular permeability, extravascular lung water is expected to increase as a result of the reduced oncotic pressure gradient between the intravascular and extravascular space. Regional and extravascular lung water is expected to increase also when pulmonary vascular permeability is intact but hydrostatic pressure within the pulmonary capillaries is increased, however, as in cardiogenic pulmonary edema or volume overload (21). A more specific measure of pulmonary vascular permeability may be derived by measuring, with PET, the transport rate constants (pulmonary transcapillary escape rate) of a radiolabeled protein, such as ^{68}Ga-transferrin or ^{11}C-methylalbumin, between the intravascular and the extravascular space (20, 22).

PET IMAGING OF ACUTE LUNG INJURY

Acute respiratory distress syndrome and acute lung injury have traditionally been considered as the expression of a diffuse inflammatory process that involves the pulmonary parenchyma. Sandiford and coworkers (23) reported that pulmonary vascular permeability, measured *in vivo* from the pulmonary transcapillary escape rate of ^{68}Ga-transferrin, was higher in patients with acute respiratory distress syndrome than in normal subjects, and within the acute respiratory distress syndrome group, they did not find consistent differences in pulmonary transcapillary escape rate between ventral and dorsal lung regions. They reported that extravascular lung density was significantly higher in dorsal, dependent regions, however, than in ventral, nondependent ones. These data suggest that even when the inflammatory process is not confined to dependent lung regions, the resulting increase in lung density may be heterogeneously distributed and predominantly dependent. Although it may seem obvious that nonaerated regions represent regions of shunt, the extent to which these regions contribute to the impairment of gas exchange depends on their perfusion. A recent study that used PET imaging of $H_2{}^{15}O$ to measure regional pulmonary blood flow showed only minimal redistribution of pulmonary perfusion away from regions of edema in patients with acute respiratory distress syndrome and acute lung injury, suggesting that mechanisms that preserve ventilation–perfusion matching, such as hypoxic pulmonary vasoconstriction, are severely blunted in these patients and that perfusion to edematous regions is substantial (21). The ability of compensatory mechanisms to preserve ventilation–perfusion matching may depend on the pathophysiology of the injury, however, and the most effective means to ameliorate gas exchange will likely depend on which underlying pathophysiologic phenomenon is prevalent (24). Using PET imaging of $^{13}N_2$ in an experimental model of lung injury, the authors showed that, when shunt in poorly aerated but recruitable lung regions was the predominant mechanism of impairment of gas exchange, positive end-expiratory pressure restored aeration and reduced shunt in these regions (25). In contrast, when sustained lung inflation was not accompanied by stable and substantial alveolar recruitment, increased airway pressure worsened gas exchange by diverting blood flow from more aerated to less aerated regions, with the consequence that a larger fraction of pulmonary perfusion was shunted in poorly aerated regions (7). In this situation, interventions aimed at manipulating regional pulmonary perfusion, such as inhaled pulmonary vasodilators with or without intravenous pulmonary vasoconstrictors (26–28), could be more effective means to improve gas exchange than increased airway pressure.

An intervention that can lead to improvement of gas exchange without concomitant increase in airway pressure is prone positioning. Using PET imaging of $^{13}N_2$, the authors investigated the effect of prone positioning on the regional distribution of pulmonary perfusion, shunt, aeration, and ventilation in a surfactant-deficient model of lung injury induced by saline lung lavage (29). The authors showed that the improvement of gas exchange in the prone position was associated with restored aeration and reduced shunt in dorsal lung regions, without a concomitant reduction of aeration and increase of shunt in ventral regions (Figure 2 [p. 508]). As a result, the distribution of lung gas volume became more uniform in the prone position. The beneficial effect that the improvement of regional aeration had on regional gas exchange was apparent from the relation between regional shunt and gas fraction (Figure 6 in Reference 29). This relation showed that the effect of the prone position was to shift dorsal regions to a more favorable portion of the shunt versus gas fraction relation. Interestingly, in five animals, the authors observed a biphasic behavior, with low shunt fraction in regions with gas fraction higher than a critical threshold ($\sim$ 0.35) and a steep linear increase of shunt in regions with gas fraction lower than this threshold. This finding suggests that even regions with reduced aeration maintain the ability to exchange gas, provided that aeration remains above a critical threshold. Furthermore, assuming that shunt fraction is proportional to the fraction of derecruited units, the linear increase of shunt for gas fraction lower than a threshold is consistent with a "quantal" loss of gas-exchanging units during alveolar derecruitment: the decrease in aeration of a region is absorbed only by a certain number of its units that become atelectatic and lose the ability to exchange gas, whereas the remaining units preserve their aeration and, accordingly, their gas exchange. The improvement of gas exchange in the prone position was further enhanced by the fact that perfusion to dorsal regions remained substantial even in this position, allowing these regions to take advantage of their restored aeration and leading to an increase of dorsal, and total, gas-exchanging pulmonary blood flow (Figure 2). These observations emphasize the importance of assessing regional perfusion, ventilation, and shunt to elucidate thoroughly the pathophysiologic basis of the gas exchange response to different interventions in acute respiratory distress syndrome and acute lung injury.

In an acute smoke inhalation injury model, Willey-Courand and coworkers (30) used PET imaging of $^{13}N_2$ to show that, in the early hours after smoke inhalation, substantial shunt developed in dependent lung regions, where gas fraction decreased and perfusion was highest. As a result of the high perfusion and high shunt fraction in dependent regions, a large fraction of pulmonary blood flow went to shunting units in these regions, leading to systemic hypoxemia.

PET IMAGING OF PULMONARY EMBOLISM WITH $^{13}N_2$

In an experimental model of autologous blood clot pulmonary embolism, the authors used PET imaging of $^{13}N_2$ to assess changes in regional perfusion and ventilation (9). After acute pulmonary embolism, both the perfusion-weighted and the ventilation-weighted distributions of ventilation–perfusion ratio became significantly broader than at baseline, although they remained unimodal (10). After embolism, specific alveolar ventilation of lung regions that remained perfused, measured from the washout rate of infused $^{13}N_2$, increased significantly compared with baseline, despite constant ventilatory settings. Furthermore, PET imaging of inhaled $^{13}N_2$ allowed determination of specific ventilation of embolized regions, in which the washout rate of inhaled $^{13}N_2$ decreased after embolism and was lower than that of regions that remained perfused (9). Taken together, these results suggest that acute pulmonary embolism is accompanied by a shift of ventilation from embolized regions toward regions with preserved perfusion. This shift is probably caused by hypocapnic pneumoconstriction in embolized regions and represents a homeostatic mechanism that aims at reducing ventilation–perfusion mismatch caused by pulmonary embolism.

PET IMAGING OF BRONCHOCONSTRICTION WITH THE $^{13}N_2$–SALINE BOLUS INFUSION TECHNIQUE

The authors recently applied PET imaging of infused $^{13}N_2$ to assess regional perfusion, ventilation, and gas trapping in animal models of acute bronchoconstriction and in subjects with asthma. In these studies of methacholine-induced bronchoconstriction, they demonstrated the presence of large regions of lung that retained $^{13}N_2$ during the washout phase after the bolus infusion of $^{13}N_2$–saline. These regions represent areas that were perfused but severely hypoventilated. The perfusion-weighted distribution

of ventilation–perfusion ratio, derived by PET, showed a bimodal profile, whereby units with low ventilation–perfusion ratio received a substantial fraction of perfusion (10). Vidal Melo and coworkers (31) demonstrated that the bimodality of the ventilation–perfusion distribution during bronchoconstriction was partly caused by heterogeneity occurring at small scales, lower than the spatial resolution of PET, in addition to the contribution of the effect of large regions of tracer retention easily visualized on the PET scan. When intraregional washout kinetics was analyzed with a single compartment model, bimodal ventilation–perfusion distributions were derived for half of the six bronchoconstricted animals studied, suggesting that, in these three animals, *interregional* heterogeneity at scales greater than 2.2 cm^3 (the effective resolution volume of the images) accounted for at least part of the bimodality of the ventilation–perfusion distribution. The presence of significant *intraregional* heterogeneity, however, occurring within the resolution volume, was revealed by curvilinear semilogarithmic $^{13}N_2$ washout kinetics in a large number of voxels. Accordingly, the heterogeneity derived from a double compartment model analysis of the tracer kinetics of each voxel was greater than that derived from a single compartment model, indicating that significant heterogeneity of ventilation–perfusion ratio was present at scales lower than the spatial resolution of the images. Indeed, the heterogeneity of the ventilation–perfusion distribution derived without accounting for intraregional heterogeneity (i.e., single compartment model) underestimated by 38% the global (i.e., intraregional plus interregional) heterogeneity derived from the double compartment model. These results demonstrate how, despite being unable to localize topographically ventilation–perfusion heterogeneity at scales lower than the spatial resolution of PET, the $^{13}N_2$–saline bolus infusion technique allows detection and quantification of a substantial amount of functionally relevant subresolution heterogeneity of ventilation–perfusion ratio, because application of a double compartment model to the washout kinetics of infused $^{13}N_2$ allows estimation not only of ventilation of the fast and slow compartments but also of the fraction of perfusion to each compartment, being tracer partitioning between the two compartments at the beginning of the washout proportional to their relative perfusion. In this sense, the $^{13}N_2$ kinetic information derived from the sequence of PET frames (i.e., temporal resolution) allows quantification of heterogeneity of ventilation–perfusion ratio that occurs at scales lower than the spatial resolution of PET, although the topographic localization of such heterogeneity remains elusive. Only after this small-scale heterogeneity of ventilation–perfusion ratio was taken into account could arterial blood gases during bronchoconstriction be closely estimated from the tracer kinetics of infused $^{13}N_2$ (10, 31).

The finding that intraregional heterogeneity was not only responsible for a significant fraction of the ventilation–perfusion mismatch but was also a main determinant of the bimodality of the ventilation–perfusion distribution supports the concept that changes in peripheral airways are largely responsible for gas exchange impairment during bronchoconstriction. These results demonstrate that one source of the bimodality of the ventilation–perfusion distribution rests within lung structures with volume smaller than 2.2 cm^3, which corresponds to the volume of a secondary pulmonary lobule (32).

Taken together, these results indicate that ventilation–perfusion distributions during experimental bronchoconstriction have two topographic components. One component results from ventilation–perfusion heterogeneity between large lung regions, of at least segmental size, which appear as clusters of tracer retaining units on the final PET frames of the washout. The second component is caused by intraregional heterogeneity within lung structures with volume lower than 2.2 cm^3 and probably results from bistable terminal bronchiolar constriction (33). This subresolution heterogeneity proved essential to quantify gas exchange alterations during experimental bronchoconstriction.

As in the animal model of bronchoconstriction, large clusters of poorly ventilated lung units were detected with PET in subjects with asthma (Figure 3 [p. 509]). To explain these results, the authors formulated a theoretic model that incorporates the effects of tidal stretch on smooth muscle, the interdependence between airway wall and parenchymal forces, and the branching structure of the tracheobronchial tree (15). Despite a nearly symmetric bronchial tree structure and smooth muscle activation imposed on the model, constriction of the tree leads to self-organized patchiness of ventilation (Figure 4, *background* [p. 509]). In this model, as smooth muscle tone is increased, an initially uniform distribution of ventilation gives rise to a catastrophic, stepwise development of clusters of hypoventilated units, with the clusters growing in size as smooth muscle tone increases, whereas the rest of the lung maintains normal and uniform ventilation. Consistent with the PET data, the network model shows coexistence of ventilated and poorly ventilated terminal units within the clusters, and predicts that cluster size and number of severely constricted terminal bronchioles increase with decreasing tidal volume. This model suggests that in severe asthma, as increased respiratory effort and fatigue reduce tidal volume and parenchymal expansion, an increasing part of the lung becomes exposed to catastrophic airway closure (Figure 4, *foreground*), a process that without treatment is likely to lead to respiratory failure. Clustered bronchoconstriction could also limit the effectiveness of inhaled therapeutic drugs for asthma by promoting their delivery to lung regions least in need of medication. Indeed, delivering bronchodilatory medication to regions that remain well ventilated could divert an even greater fraction of ventilation toward them, further reducing lung expansion of constricted areas and exacerbating ventilation heterogeneity. This heterogeneous pattern of constriction could explain the ineffectiveness of inhaled bronchodilators in some patients, and the need to deliver bronchodilators through the vascular system in some cases of severe asthma (34). It is possible that the potential for catastrophic shifts in airway constriction and the clustered distribution of airway obstruction are involved in sudden and unexplained asthma attacks that are usually difficult to treat.

Several other techniques have been used to image bronchoconstricted lungs. Scintigraphic ventilation and perfusion scans have demonstrated ventilation and perfusion heterogeneity in mild asthmatics, but at a spatial resolution not sufficient to assess its functional significance. High-resolution CT has provided distinct anatomic information on the constriction of airways with diameter greater than 2 mm (35) and has been used to assess the presence and location of gas trapping after an exhalation to residual volume (36). SPECT with Technegas has been used to assess airway closure in subjects with asthma, although this technique is unlikely to detect changes in lung regions with volume lower than 51 ml (37). More recently, MRI with ^3He has allowed high-resolution visualization of ventilation defects in symptomatic and asymptomatic subjects with asthma (38).

In conclusion, we have illustrated with several examples how functional lung imaging with PET provides valuable insights into the pathophysiology of several pulmonary processes and is an attractive method to quantify regional gas exchange thoroughly in clinical and experimental research, and, possibly in the future, in clinical practice.

Conflict of Interest Statement: G.M. does not have a financial relationship with a commercial entity that has an interest in the subject of this manuscript. J.G.V. is coinvestor of (patent 674137) a device to proance and inject nitrogen-13 in saline solution. The patent is assigned to the General Hospital Corporation (Boston, MA) and is not licensed commercially.

Acknowledgment: The authors thank Marcos F. Vidal Melo, M.D., Ph.D., for insightful comments.

References

1. Rhodes CG, Valind SO, Brudin LH, Wollmer PE, Jones T, Hughes JMB. Quantification of regional V/Q ratios in humans by the use of PET. I. Theory. *J Appl Physiol* 1989;66:1896–1904.
2. Rhodes CG, Valind SO, Brudin LH, Wollmer PE, Jones T, Buckingham PD, Hughes JMB. Quantification of regional V/Q ratios in humans by the use of PET. II. Procedure and normal values. *J Appl Physiol* 1989;66:1905–1913.
3. Mijailovich SM, Treppo S, Venegas JG. Effects of lung motion and tracer kinetics corrections on PET imaging of pulmonary function. *J Appl Physiol* 1997;82:1154–1162.
4. Musch G, Layfield JDH, Harris RS, Vidal Melo MF, Winkler T, Callahan RJ, Fischman AJ, Venegas JG. Topographical distribution of pulmonary perfusion and ventilation, assessed by PET in supine and prone humans. *J Appl Physiol* 2002;93:1841–1851.
5. Galletti GG, Venegas JG. Tracer kinetic model of regional pulmonary function using positron emission tomography. *J Appl Physiol* 2002; 93:1104–1114.
6. O'Neill K, Venegas JG, Richter T, Harris RS, Layfield JDH, Musch G, Winkler T, Vidal Melo MF. Modeling kinetics of infused ^{13}NN-saline in acute lung injury. *J Appl Physiol* 2003;95:2471–2484.
7. Musch G, Harris RS, Vidal Melo MF, O'Neill KR, Layfield JDH, Winkler T, Venegas JG. Mechanism by which a sustained inflation may worsen oxygenation in acute lung injury. *Anesthesiology* 2004;100:323–330.
8. Valind SO, Wollmer PE, Rhodes CG. Application of positron emission tomography in the lung. In: Reivich M, Alavi A, editors. Positron emission tomography. New York: Liss; 1985. pp. 387–412.
9. Vidal Melo MF, Harris RS, Layfield D, Musch G, Venegas JG. Changes in regional ventilation after autologous blood clot pulmonary embolism. *Anesthesiology* 2002;97:671–681.
10. Vidal Melo MF, Layfield D, Harris RS, O'Neill K, Musch G, Richter T, Winkler T, Fischman AJ, Venegas JG. Quantification of regional ventilation-perfusion ratios with PET. *J Nucl Med* 2003;44:1982–1991.
11. Kreck TC, Krueger MA, Altemeier WA, Sinclair SE, Robertson HT, Shade ED, Hildebrandt J, Lamm WJ, Frazer DA, Polissar NL, *et al.* Determination of regional ventilation and perfusion in the lung using xenon and computed tomography. *J Appl Physiol* 2001;91:1741–1749.
12. Eberle B, Weiler N, Markstaller K, Eberle B, Kauczor H, Deninger A, Ebert M, Grossmann T, Heil W, Lauer LO, *et al.* Analysis of intrapulmonary O_2 concentration by MR imaging of inhaled hyperpolarized helium-3. *J Appl Physiol* 1999;87:2043–2052.
13. Rizi RR, Baumgardner JE, Ishii M, Spector ZZ, Edvinsson JM, Jalali A, Yu J, Itkin M, Lipson DA, Gefter W. Determination of regional VA/Q by hyperpolarized 3He MRI. *Magn Reson Med* 2004;52:65–72.
14. Petersson J, Sanchez-Crespo A, Rohdin M, Montmerle S, Nyren S, Jacobsson H, Larsson SA, Lindahl SGE, Linnarsson D, Glenny RW, *et al.* Physiological evaluation of a new quantitative SPECT method measuring regional ventilation and perfusion. *J Appl Physiol* 2004; 96:1127–1136.
15. Venegas JG, Winkler T, Musch G, Vidal Melo MF, Layfield D, Tgavalekos N, Fischman AJ, Callahan RJ, Bellani G, Harris RS. Self-organized patchiness in asthma as a prelude to catastrophic shifts. *Nature* 2005;434:777–782.
16. Richard JC, Janier M, Lavenne F, Tourvieille C, Le Bars D, Costes N, Gimenez G, Guerin C. Quantitative assessment of regional alveolar ventilation and gas volume using ^{13}N-N_2 washout and PET. *J Nucl Med* 2005;46:1375–1383.
17. Simon BA, Venegas JG. Analyzing ^{13}NN lung washout curves in the presence of intraregional nonuniformities. *J Appl Physiol* 1994;76:956–964.
18. Mintun MA, Ter-Pogossian MM, Green MA, Lich LL, Schuster DP. Quantitative measurement of regional pulmonary blood flow with positron emission tomography. *J Appl Physiol* 1986;60:317–326.
19. Schuster DP, Kaplan JD, Gauvain K, Welch MJ, Markham J. Measurement of regional pulmonary blood flow with PET. *J Nucl Med* 1995;36: 371–377.
20. Schuster DP. Positron emission tomography: theory and its application to the study of lung disease. *Am Rev Respir Dis* 1989;139:818–840.
21. Schuster DP, Anderson C, Kozlowski J, Lange N. Regional pulmonary perfusion in patients with acute pulmonary edema. *J Nucl Med* 2002; 43:862–870.
22. Schuster DP, Markham J, Welch MJ. Positron emission tomography measurements of pulmonary vascular permeability with ^{68}Ga-transferrin or ^{11}C-methylalbumin. *Crit Care Med* 1998;26:518–525.
23. Sandiford P, Province MA, Schuster DP. Distribution of regional density and vascular permeability in the adult respiratory distress syndrome. *Am J Respir Crit Care Med* 1995;151:737–742.
24. Gust R, McCarthy TJ, Kozlowski J, Stephenson AH, Schuster DP. The response to inhaled nitric oxide in acute lung injury depends on the distribution of pulmonary blood flow prior to its administration. *Am J Respir Crit Care Med* 1999;159:563–570.
25. Musch G, Bellani G, O'Neill KR, Harris RS, Vidal Melo MF, Winkler T, Venegas JG. Functional PET imaging of the effect of PEEP on regional gas exchange in acute lung injury [abstract]. *Am J Respir Crit Care Med* 2004;169:A545.
26. Bigatello LM, Hurford WE, Kacmarek RM, Roberts JD, Zapol WM. Prolonged inhalation of low concentrations of nitric oxide in patients with severe adult respiratory distress syndrome: effects on pulmonary hemodynamics and oxygenation. *Anesthesiology* 1994;80:761–770.
27. Manktelow C, Bigatello LM, Hess D, Hurford WE. Physiologic determinants of the response to inhaled nitric oxide in patients with acute respiratory distress syndrome. *Anesthesiology* 1997;87:297–307.
28. Roch A, Papazian L, Bregeon F, Gainnier M, Michelet P, Thirion X, Saux P, Thomas P, Jammes Y, Auffray JP. High or low doses of almitrine bismesylate in ARDS patients responding to inhaled NO and receiving norepinephrine? *Intensive Care Med* 2001;27:1737–1743.
29. Richter T, Bellani G, Harris RS, Vidal Melo MF, Winkler T, Venegas JG, Musch G. Effect of prone position on regional shunt, aeration and perfusion in experimental acute lung injury. *Am J Respir Crit Care Med* 2005;172:480–487.
30. Willey-Courand DB, Harris RS, Galletti GG, Hales CA, Fischman A, Venegas JG. Alterations in regional ventilation, perfusion, and shunt after smoke inhalation measured by PET. *J Appl Physiol* 2002;93: 1115–1122.
31. Vidal Melo MF, Harris RS, Layfield JDH, Venegas JG. Topographic basis of bimodal ventilation-perfusion distributions during bronchoconstriction in sheep. *Am J Respir Crit Care Med* 2005;171:714–721.
32. Itoh H, Nakatsu M, Yoxtheimer LM, Uematsu H, Ohno Y, Hatabu H. Structural basis for pulmonary functional imaging. *Eur J Radiol* 2001; 37:143–154.
33. Anafi RC, Wilson TA. Airway stability and heterogeneity in the constricted lung. *J Appl Physiol* 2001;91:1185–1192.
34. Smith D, Riel J, Tilles I, Kino R, Lis J, Hoffman JR. Intravenous epinephrine in life-threatening asthma. *Ann Emerg Med* 2003;41:706–711.
35. Brown RH, Mitzner W. Understanding airway pathophysiology with computed tomography. *J Appl Physiol* 2003;95:854–862.
36. Lynch DA, Newell JD, Tschomper BA, Cink TM, Newman LS, Bethel R. Uncomplicated asthma in adults: comparison of CT appearance of the lungs in asthmatic and healthy subjects. *Radiology* 1993;188:829–833.
37. King GG, Eberl S, Salome CM, Young IH, Woolcock AJ. Differences in airway closure between normal and asthmatic subjects measured with single-photon emission computed tomography and Technegas. *Am J Respir Crit Care Med* 1998;158:1900–1906.
38. Altes TA, Powers PL, Knight-Scott J, Rakes G, Platts-Mills TA, de Lange EE, Alford BA, Mugler JP, Brookeman JR. Hyperpolarized ^{3}He MR lung ventilation imaging in asthmatics: preliminary findings. *J Magn Reson Imaging* 2001;13:378–384.